Self-Assembling Behavior of Butadienyllithium Headgroups in Benzene via SANS Measurements

Jörg Stellbrink,*,† Lutz Willner, and Dieter Richter

Institut für Festkörperforschung, Forschungszentrum, Jülich GmbH, D-52425 Jülich, Germany

Peter Lindner

Institute Laue-Langevin, 156 Avenue des Martyrs, F-38042 Grenoble, Cedex 9, France

Lewis J. Fetters and John S. Huang‡

Exxon Research and Engineering Company, Corporate Research Laboratories, 1545 Rt. 22 East, PO Box 998, Annandale, New Jersey 08801-0998

Received November 18, 1998; Revised Manuscript Received May 4, 1999

ABSTRACT: The self-assembling behavior of butadienyllithium (−CH_2−CH═CH−CH_2−Li) headgroups in benzene has been studied via the use of small-angle neutron scattering (SANS). The carrier polystyrene chain molecular mass was 2.6K. Previous work has shown that the styryllithium headgroup can simultaneously form aggregated architectures encompassing tetramers and dimers along with a small number, ∼0.1%, of chains engaged in the formation of large scale mass fractal aggregates. That aggregation behavior contradicts the long entrenched belief that the sole self-assembled state of styryllithium headgroups is dimeric. This study shows that the butadienyllithium active centers exhibit more complicated aggregation tendencies than their styryllithium counterparts. For example, the butadienyllithium headgroup can form star-shaped structures with mean functionalities as large as 10 in addition to dimers. This structural versatility is in obvious conflict with the current propagation model that requires tetramers as the solitary aggregation state.

Introduction

The living character of organolithium-based anionic polymerizations involving diene or styrenic monomers conducted in hydrocarbon solvents have facilitated the synthesis of numerous polymers of varying architecture and composition. In contrast, though, important chain-growth-related questions remain. This is a consequence of the capacity of the highly ionic lipophobic headgroups to undergo self-assembly in hydrocarbon solvents. These monofunctional chains are thus a subgroup of the broad class of associating polymers and surfactants that contain a small fraction of strongly interacting groups (the stickers) which form aggregates varying in size and architecture with *n* stickers per aggregated polymer brush[1].

The textbook view[2−15] of chain propagation requires the belief that aggregation breeds dormant organolithium headgroups[16] and, as a necessary corollary, the notion that the singlet headgroups are the solitary practitioners of chain growth. The latter are assumed to emerge briefly via dissociation of their aggregated counterparts. This sequence demands, in turn, compliance with the conjecture that the inverse of the propagation reaction order (taken as $^1/_4$ or $^1/_2$)[17] directly yields the association state of these organolithium headgroups. Thus, butadienyllithium is strictly limited to four stickers per aggregate[18,19] while the styryllithium limit is taken to be two. SANS results[20] have demonstrated that this latter headgroup can also form tetramers: a result in disagreement with the above interpretation.

This paper will focus on the association behavior of butadienyllithium active centers where headgroup concentrations were varied. The major structures found are dimers and star-shaped aggregates along with a small fraction (∼0.7% of the headgroups) of larger scale structures.

Experimental Section

Sample Preparation and Evaluation. The basic high vacuum practices followed in this work for monomer and solvent purification and those procedures involving the initiator (*sec*-butyllithium) and polymer preparation and characterization have been previously given.[20−22] Following the h_{10}-styrene polymerization, d_6-butadiene was added to generate the butadienyllithium active center. Polymer concentrations were less than Φ^*, the volume fraction overlap concentration. This parameter emerges from the term $3M_w/(N_a 4\pi R_g^3)$ where the dimer M_w was used.

These active solutions were then captured in the tubular part of the quartz cell unit of the reactor and stored at ca. −15° C. The 0.5 mm path length quartz cells were used. Storage of the frozen solutions in the quartz cells is not recommended since thawing can lead to cell rupture. Sample nomenclature follows that used previously.[20,22] The base polystyrene chain is given along with the headgroup. Thus the sample SBdLi(2.6) describes the polystyrene chain with the molecular mass of 2.6K and capped with the butadienyllithium headgroup. This base polystyrene chain was that used for the previous[20] aggregation state assay of the styryllithium headgroup. The volume fraction of polymer in each solution was obtained from the SANS measurements. These concentrations were no greater ±4% with regard to the stoichiometric values.

SANS. Small-angle neutron scattering (SANS) directly investigates in microscopic detail the scattering units with a resolution of several angstroms. It is thus the ideal tool for

* To whom correspondence should be addressed.

† Present address: Department of Physics and Astronomy, James Clerk Maxwell Bldg., Edinburgh University, Edinburgh EH9 3JZ, U.K. E-mail: j.stellbrink@ed.ac.uk

‡ Present address: Department of Materials Science, Princeton University, Princeton, NJ 08544

10.1021/ma9817931 CCC: $18.00
Published on Web 07/02/1999

evaluating the structural characteristics of the intermediate-sized aggregates found in this work since their length scales r fall within the instrumental Q range (r and Q are inversely related). The parameter Q, the scattering vector, is given by $4\pi[\sin(\theta/2)]\lambda^{-1}$ with θ the scattering angle and λ the neutron wavelength. The SANS measurements were done on the D-11 instrument at the Institute Laue-Langevin (ILL), Grenoble, France. Detector settings of 2, 10, and 35.7 m were used. A neutron wavelength of $\lambda = 7$ Å was used, and the spread was $\Delta\lambda = 14\%$. This wavelength led to an experimental Q range of 1.32×10^{-3} to 0.16 Å^{-1}. The macroscopic coherent scattering cross section $d\Sigma/d\Omega$ from polymers in solution is given by

$$\frac{d\Sigma}{d\Omega} = \frac{\Delta\rho^2}{N_A}\frac{\Phi(1-\Phi)}{\left[\frac{1}{V_w P(Q)} + 2A_2\Phi\right]} \quad (1)$$

where Φ denotes the polymer volume fraction, $P(Q)$ the form factor of the polymer or the polymer aggregates, V_w the corresponding weight average molar polymer volume, A_2 the second virial coefficient, and N_A the Avogadro number and $\Delta\rho = [(\Sigma b_s/v_s) - (\Sigma b_{mon}/v_{mon})]$ is the scattering contrast. The ratio $\Sigma b_s/v_s$ is the scattering length density of the solvent while b_s denotes the scattering lengths of the atoms forming the solvent molecule and v_s is the corresponding volume. $\Sigma b_{mon}/v_{mon}$ is the corresponding quantity for the monomer unit.

In general all radially averaged D11 data were normalized to a water standard. In addition the 2-meter data from the D11 instrument were corrected for detector dead time effects. Contributions due to incoherent background and solvent scattering were subtracted from all data sets. The SANS measurements were performed at room temperature. The protocols of instrumental calibrations and the data evaluation procedures are given in ref 20.

Model Form Factors. For the following we introduce the notion of the scattering function $I(Q) = (N_A/\Delta\rho^2)(d\Sigma/d\Omega)$. The molecular volume and the virial coefficients are obtained from $I(Q)$ e.g., in terms of the Zimm[23] approximation where $I(Q)$ is simultaneously extrapolated to $Q \rightarrow 0$ and $\Phi \rightarrow 0$. To account for the complete Q dependence at finite polymer concentrations, the explicit form factor of the scattering particles is needed. This parameter has been calculated analytically for special polymer architectures. In our recent publication on living polymerizations[20] we showed that in different Q regimes the scattering profiles from polystyryllithium could be well described by the following form factors. At low-Q the mass fractal form factor by Beaucage[24−26] led to good fits while at the mid- and high-Q values the data were well described by in terms of the form-factors for Gaussian linear chains (Debye[27]) and f_w functional Gaussian stars (Benoit[28]).

The Beaucage form factor[24−26] is valid for arbitrary mass fractals and may also be applied to polymeric systems. The function describes one fractal unit and is given by a sum of two contributions: (i) the first has the Guinier form and gives the overall scattering while (ii) the second deals with the power law scattering from a fractal including the proper crossover properties. For fractal structures that are themselves built of subunits, which also have fractal character, a second set of functions has to be added for a proper description of the subunit. Hence, we have

$$I(Q) = \phi(1-\phi)\left[Ge^{(-Q^2R_g^2/3)} + B\cdot e^{(-Q^2R_s^2/3)}\left(\frac{1}{Q^*}\right)^P + G_s e^{(-Q^2R_s^2/3)} + B_s\left(\frac{1}{Q_s}\right)^{P_s}\right] \quad (2)$$

with $Q^* = Q/[\mathrm{erf}(QR_g k/\sqrt{6})]^3$ and $Q_s^* = Q/[\mathrm{erf}(QR_s k/\sqrt{6})]^3$. G, B, G_s, and B_s are amplitudes, and erf denotes the error function. R_g and R_s stand for the radii of gyration and P and P_s for the fractal dimensions for the overall structure and the subunits, respectively. The amplitudes may be related with respect to each other, where $B = GPR_g^P\Gamma(P/2)$ (polymeric constraint); Γ is the gamma function, and k is an empirical constant, where $k = 1.06$. G_s and B_s are related equivalently. If the length scales R_g and R_s are well-separated, two power law regimes in Q with exponents P and P_s evolve. For mass fractals the exponents may assume values[29] between 1 and 3. The gradient of 1 denotes the rodlike posture, 2 the Debye chain[27]while a P between 2 and 3 is characteristic for more dense mass fractal structures.[29]

One of the simpler nonlinear architectures is that of polymer stars having symmetric arms with a functionality of f_w. Benoît[28] calculated the form factor for the Gaussian star:

$$P_{star}(Q) = \frac{2}{f_w Q^4 R_{g,arm}^4}\left[Q^2R_{g,arm}^2 - (1 - e^{-Q^2R_{g,arm}^2}) + \frac{f_w - 1}{2}(1 - e^{-Q^2R_{g,arm}^2})^2\right] \quad (3)$$

The scattering profile in the mid-Q regime (0.02 Å^{-1} < Q < 0.2 Å^{-1}) for the styryllithium headgroup was successfully modeled[20] in terms of a dimer−tetramer mixture over the concentration range 2.6−9.4 vol %. To account for the respective scattering profiles, eq 1 had to be generalized in order to incorporate the scattering from two different species: tetramers and dimers. Thus, the tetramer scattering was described by eq 3 while the dimers were modeled in terms of a Debye function,[27] $P_{Debye}(Q)$. With this eq 1 assumes the form

$$I(Q) = \frac{\Phi(1-\Phi)}{1/(\Phi_{rel}^{star}V_{star}P_{star}(Q) + (1 - \Phi_{rel}^{star})V_{dim}P_{Debye}(Q)) + 2A_2\Phi} \quad (4)$$

with $\Phi_{rel}^i = \Phi_i/\Phi$ and Φ_i the volume fraction of component i.

Second Virial Coefficients. The application of eq 1 and the derived eq 4 requires knowledge of A_2. For polystyrene based on literature[30] for $M_w > 5 \times 10^4$ g mol^{-1} the relation $A_2 = 0.0106M_w^{-0.26}$ (ml mol g^{-2}) holds. On the other hand for smaller molecular masses, Burchard et al.[31] found larger values for A_2 than projected by the relation above. These data together with our recent SANS results lead to $A_2 = 0.024\ (\pm 0.005)M_w^{-0.30(\pm 0.07)}$ (ml mol g^{-2}). Star polymers exhibit a different virial coefficient than linear chains of identical M_w. The conversion between the respective values obeys $A_{2,star} = g_A A_{2,linear}$ with M_w (star) = M_w (linear). Roovers[32] has collected g_A values for various functionalities. For star functionalities up to 18 they can be represented by $g_A = (1.09 \pm 0.08) - (0.04 \pm 0.007)f_w$. Using this relation allows for a proper consideration of an architecture dependent virial coefficient in eq 1 or 4.

Results

Generic Scattering Behavior. To display the general quality of the data, as well as the orders of magnitudes of the cross sections, Figure 1 displays scattering data taken at the lowest polymer volume fraction $\Phi = 0.54\%$ for the living and terminated chains and compares them with the solvent scattering. Note that here, in contrast to the protocol used in the following SANS figures, the solvent scattering has not been subtracted from the polymer data. Furthermore, all solutions evaluated used purified benzene from the same source on the vacuum line. Thus the Figure 1 data sets are raw results that are corrected only for empty cell scattering and background. The data are normalized to a water standard according to eq 5 of ref 20. We first note that even at this low volume fraction, given the short chain lengths we are investigating, the signal from the terminated chains is still well above the solvent scattering with the Guinier plateau at about twice the solvent level. The intensity profile from the terminated chains follows typical Debye behavior. Compared to the terminated system, the scattering from the living poly-

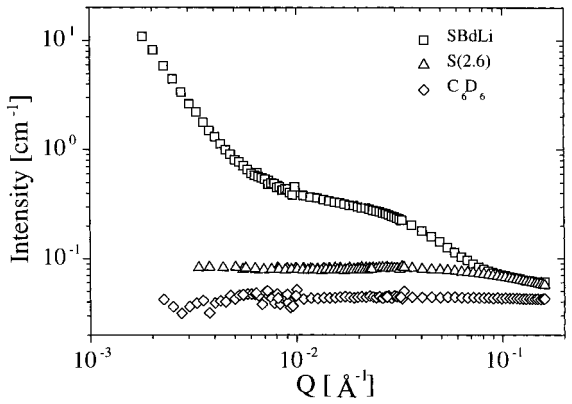

Figure 1. Scattering intensity (raw data) vs scattering vector Q for the terminated polystyrene sample and the corresponding living polymer SBdLi ($\Phi = 0.54\%$). Also shown are the data of the pure solvent C_6D_6.

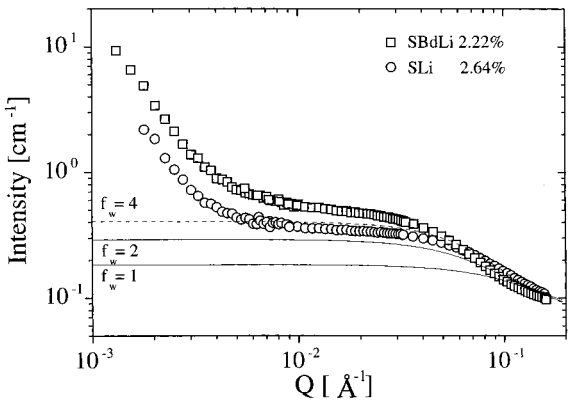

Figure 2. $I(Q)$ for the living polymers SBdLi (□) and SLi (○). The lines denote the calculated $I(Q)$ for the terminated chain and the dimer (SLi) and tetramer (SBdLi) structures.

mers is strongly enhanced. Only at high-Q does it coincide with that from the terminated solution. At intermediate and lower-Q a strong enhancement of scattering is observed indicating the presence of objects with large scattering volumes: eq 1. These scattering volumes are clearly absent both in the solvent and the terminated solutions. Similarly, static light scattering measurements ($\lambda = 633$ nm) of a terminated solution (see Figure 7 of ref 22) over the Q-range of 7.5×10^{-4} to 2.9×10^{-3} Å^{-1} showed only the Q-independent scattering of objects much smaller than the wavelength of light. This combination of results shows that the increases in intensity in the mid- to low-Q regime reflect the polymeric structures formed by the self-assembling headgroups and thus are not caused, as has been alleged,[14] by the presence of suspended particulate matter.

After having displayed the significance of the scattering data, we now present a qualitative comparison with previous data[20] from the styryllithium system. Figure 2 presents scattering results at about the same volume fraction of SLi ($\Phi = 2.64\%$) and SBdLi ($\Phi = 2.22\%$). As may be seen, though, while the volume fraction of the SBdLi system is lower than its SLi counterpart its scattering is significantly above the profile from the SLi solution. Without any evaluation this direct comparison shows the higher degree of association for the butadienyllithium headgroup compared to the styryllithium system.

To quantitatively compare this scattering behavior the form factors[28] for starlike aggregates of different

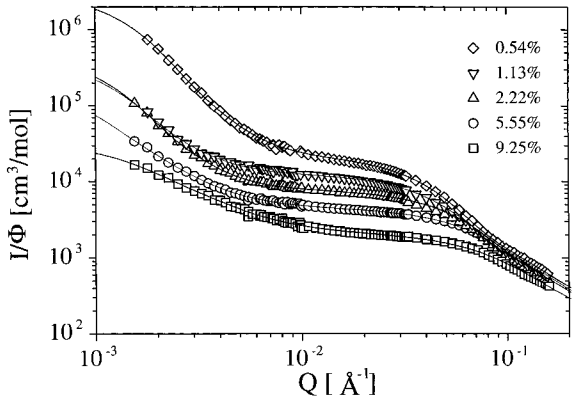

Figure 3. Fits of I/Φ for the living polymer SBdLi solutions to the mass fractal form factor.

functionalities must be considered. Thus, Figure 2 also includes the scattering profile predictions for singlet, dimeric and tetrameric chains. While in the mid-Q range the SLi system scatters at a level consistent with tetrameric aggregates, the SBdLi solution scattering is considerably stronger indicating high levels of aggregation. In addition both systems display strong scattering at low-Q signifying large scale aggregates. Obviously, the self-assembling capacities of these active centers are more versatile than the prevailing model permits.

Finally, Figure 3 presents the dependence of the SBdLi scattering patterns on polymer volume fraction. To present this comparison the SANS intensities in each case were divided by Φ. We note that the relative scattering is strongest at the lowest volume fraction. This is true for both the intermediate plateaus as well as for the low-Q scattering regimes. This general evolution of scattering with Φ has already been observed for the SLi system (see Figure 8 in ref 20) though it appears to be more pronounced for the SBdLi headgroups.

Beaucage Form Factor. The Beaucage form factor[24−26] can, at least in a partial sense, characterize the large-scale structures. Complete characterization is impossible since the $I(Q)$ profile captured by SANS is made incomplete by the failure to reach the Zimm regime. The access of that scattering vector regime requires the wavelengths (436−690 nm) and the angular range (10−160°) available in modern light-scattering instrumentation. Despite these limitations, some insight can be gleaned regarding the format of the large structures. In particular, eq 2 allows a parametrization of the scattering patterns in terms of fractal exponents along with sizes of the two structural levels. The size of R_g of the larger unit, thereby, is a minimum value required to describe the data; larger sizes are possible. Figure 3 includes the resulting fitted curves. Obviously, very good descriptions of the data are possible. Table 1 shows the SBdLi results and also includes the earlier data[20] on SLi. As mentioned above the size parameter R_g is a minimum value and should not be taken as a real aggregate size (as the authors of refs 15 and 16 have done regarding parallel findings in ref 22).

Concerning the fractal dimensions P of the large-scale aggregates we realize that in the case of the SLi-system P stays roughly constant around $P = 3$; given the limited Q-range of observation. The error range of P is estimated to be ± 0.1. The large-scale aggregates appear to be surfaceless loose 3-dimensional structures. For SBdLi, on the other hand, there seems to be a systematic reduction of P with increasing Φ indicating more open

Table 1. Results of Fitting the 0.01−0.08 Å^{-1} *Q*-Range with the Benoît Gaussian Star Form Factor, the Combined Debye/Benoît Form Factor, and the Complete *Q*-Range to the Beaucage Form Factor[a]

$10^2\Phi$	0.54	1.13	2.22	*2.64*	*5.20*	5.55	*7.05*	9.25	*9.40*
$10^{-2}[PLi]_0$ (M)	0.22	0. 45	1.1	*1.3*	*2.1*	2.3	*2.9*	3.8	*3.9*
				Benoit/Debye					
f_w	10.7 (±0.3)	6.9 (±0.3)	5.6 (±0.3)	*2.9 (±0.01)*	*2.8 (±0.01)*	4.4 (±0.1)	*2.7 (±0.02)*	3.3 (±0.1)	*2.2 (±0.02)*
R_g^{Star} **(Å)**	45 (±0.9)	39 (±1.0)	35 (±1.3)	*27 (±0.2)*	*26 (±0.1)*	32 (±1.0)	*26 (±1.2)*	30 (± 1.7)	*25 (±1.0)*
				Beaucage					
G (cm^3/mol)	3.06×10^6	4.3×10^5	4.9×10^5	*2.2×10^5*	*65000*	1.9×10^5	*7100*	31400	*7450*
R_g (Å)	1200	1500	1500	*1700*	*1300*	2100	*900*	1100	*900*
P	3.0	2.7	2.8	*3.0*	*3.0*	2.3	*3.0*	1.9	*2.8*
G_s (cm^3/mol)	21500	12400	7700	*4050*	*2850*	3800	*2300*	2050	*1650*
R_s (Å)	44	39	30	*22*	*19*	24	*18*	20	*14*
B_s (cm^3/mol)[b]	0.16	0.30	0.56			1.38		1.96	
P_s	1.67	1.67	1.67	*2*	*2*	1.67	*2*	1.67	*2*

[a] Italicized data (ref 20) are for SLi. [b] Use of the polymeric constraint eleminates this parameter for the SLi data.

structures as Φ increases. This is a demonstration that the large scale component of SBdLi(2.6) seemingly "melts" under conditions where the corresponding SLi(2.6) headgroup retains $P \cong 3$. This behavior is a headgroup effect, since chain lengths are identical for these systems while concentration differences are minor. The finding that P ranges from about 3 to 2 also explains why for the highest concentration of SBdLi(2.6) where P approaches 2 a fit with a Debye form factor was possible.[17] That model commences to fail as headgroup concentration diminishes, i.e., as $P > 2$. Hence, attenuation of the large scale SBdLi(2.6) structures occurs as polymer and headgroup concentrations increases.

Concerning the subunits (high-Q range) we observe two important differences between the SLi and SBdLi structures: (i) Although both subunits are built from identical base PS chains ($M_w = 2.6$K) the size of the SBdLi subunit at a given concentration is systematically larger than that of the SLi system (Table 1). This indicates a higher degree of association for the former headgroup. (ii) The larger R_s is accompanied by a smaller value for P_s. While $P_s = 2$ for SLi, indicating Gaussian statistics, $P_s = 1.67$ for SBdLi is more in accordance with a swollen chain structure. The difference may be rationalized as follows. PS chains of a molecular mass of 2.6K (and the dimer and tetramer aggregates derived therefrom) follow a Gaussian random walk even in the good solvent benzene. The approach to swollen chain statistics[33] in benzene begins to set in at $M_w > 5 \times 10^4$. If such chains aggregate to higher aggregation states (see R_s) they will undergo some chain stretching-which in return aids P_s in its approach to the swollen chain (good solvent) limit. Hence, this can also contribute to the observed differences in P_s for the two headgroups. We note that a careful inspection of Figure 2 also reveals a steeper slope in the high-Q regime for SLi compared to SBdLi. Thus, the high-Q data for both headgroups contain information that helps distinguish between the aggregation behavior of these active centers.

Finally, following eq 1 and neglecting the virial coefficient the amplitude factors G and G_s in front of the Guinier terms in eq 2 directly relate to the scattering volumes V and V_s of the large and small fractal structures, respectively. Not taking into account A_2 is only reasonable for the lowest concentrations. There, the relation between the two amplitudes may be used to scrutinize the internal consistency of the Beaucage approach for our system. If the large scale mass fractal structure of size R_g is build from small fractal building blocks of size R_s, then the scattering volumes should relate according to

$$\frac{V}{V_s} \sim \left(\frac{R_g}{R_s}\right)^P \tag{5}$$

with a proportionality factor on the order of 1. Inserting the results for $\Phi = 0.54\%$ and $\Phi = 1.13\%$ we obtain

$$\phi = 0.54\%: \quad \frac{V}{V_s} = 142; \quad \left(\frac{R_g}{R_s}\right)^p = 20400 \tag{6a}$$

and

$$\phi = 1.13\%: \quad \frac{V}{V_s} = 35; \quad \left(\frac{R_g}{R_s}\right)^p = 19000 \tag{6b}$$

In both cases eq 5 is grossly violated, even through the values inserted for R_g are lower size boundaries and the real aggregates could be considerably larger.

From this inconsistency we are forced to conclude that the picture of large scale structures built from smaller building blocks is in disagreement with the observed intensities and has to be discarded. The observed scattering patterns therefore must origin from a coexisting ensemble of a large quantity of intermediately sized objects and a small fraction of large aggregates. Qualitatively this result was communicated in our paper[20] on SLi structures.

In the following, we shall first analyze the scattering patterns from the intermediate objects. Here we have to take into account the appropriate virial coefficients applying eq 1 or eq 4, respectively. Thereafter, on the basis of the results for the intermediate structures, which we will keep fixed, we will reanalyze the low-Q scattering originating from the large objects. This procedure is justified, since according to eq 5 only a minute polymer volume fraction is actually participating in the large scale aggregates; e.g., for $\Phi = 0.54\%$, we estimate $(V/V_s)/(R_g/R_s)^P = \phi_{\text{large scale}}/(\phi - \phi_{\text{large scale}})$, where $\phi_{\text{large scale}}$ is the polymer volume fraction in the large aggregates. From this estimation, only 0.7% of the monomers participate in the large scale structures. This fraction may be neglected when evaluating the intermediate size objects.

Benoit−Debye Form Factors. While in the preceding section we have described the overall scattering patterns in terms of the Beaucage multiscale fractal form factor, we now turn our attention to the large-Q part of the data. The analysis involves the medium size aggregates that we model in terms of star form factors.

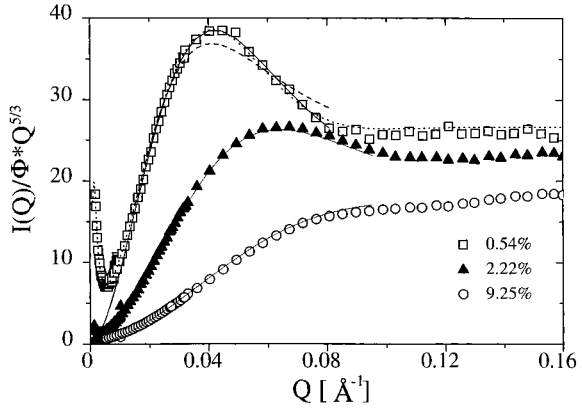

Figure 4. Kratky plots of the SBdLi headgroup with Φ = 0.54% (□), 2.2% (▲), and 9.25% (○). The Gaussian star-free fits (solid lines) yield the mean functionalities given in Table 1.

In each case we take into account the second virial parameter as given by Roovers and apply eq 1 in order to fit the data. The legitimacy of this maneuver is dependent upon the absence (or near-absence) of a continuum of aggregated structures between the star-shaped chains and those in the mass fractal format. This was the case for the SLi(2.6) headgroup[20] and the identical state of play holds for SBdLi(2.6).

The use of the Benoit Gaussian star model was strongly prompted by the progressive development in the SBdLi(2.6) scattering data (Kratky format) of the distinctive peak which has been seen earlier[34−36] for star polymers with moderate to high functionalities. An example of this can be seen in Figure 4 which presents the Φ = 0.54, 2.22, and 9.25% SBdLi(2.6) headgroup data in the Kratky format. The low concentration data presents the modeling results for the tetramer (dashed line) and the decamer counterpart. It is readily seen that the latter yields the superior fit. This peak arises in the SANS scattering profile as a consequence of the enhanced sharpness of the boundary between the star corona and the solvent. In other words, as the star approaches hard-sphere character in solution, $I(Q)$ will undergo a pronounced increase when the Q range commences to access the star dimensions, i.e., the appropriate length scale. The lesser-armed stars fail to exhibit this peak in the Kratky format simply because the star-solvent interface for low f_w (<8) stars is much more diffuse than for stars of higher functionality. Hence, the peak in the Kratky plot is a well-documented signature for the presence of star-shaped aggregates. Along this line, it should be recalled that the Kratky plot of the corresponding SLi(2.6) headgroup did not show this peak for the tetramer/dimer mixtures.[20]

An additional feature seen in Figure 4 is the low-Q upturn in $I(Q)$ for the Φ = 0.54% sample. This is a clear signal of the presence of the large-scale structures. This low-Q upturn is diminished as Φ increases. This indicates the attenuation of the large fractal structures. The previous[34−36] SANS study on stars showed that $I(Q) \rightarrow 0$ as $Q \rightarrow 0$. This is the usual behavior found for the Kratky format. The near-linear nature of the high-Q data comes from the use of $Q^{5/3}$ in the ordinate. The resultant linearity is the sign of swollen chain statistics. Interestingly, it has been found[34−36] that the Benoit model[28] is equally effective for Gaussian (its original intent) or swollen chains.

Figure 4 also includes the fit with eq 2 giving an excellent overall fit to the $I(Q)$ vs Q data (dotted line).

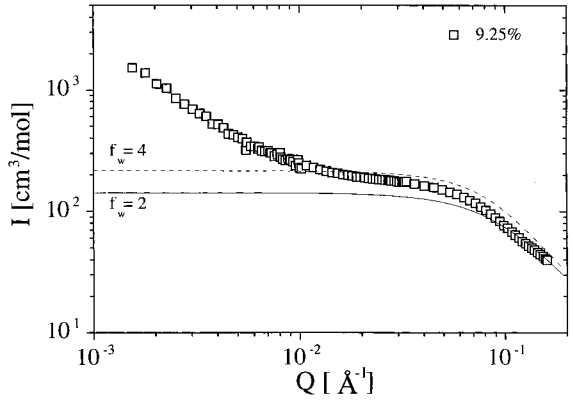

Figure 5. Gaussian star (f_w = 4) and Debye (f_w = 2) for SBdLi: Φ = 9.25%.

The Benoit form factor for Gaussian stars yields an excellent fit in the mid-Q regime; a fit in accord with the presence of star-shaped aggregates having, in this case, a mean degree functionality of about 10. Figure 5 displays star fits at the highest concentrations with the predicted form factors for f_w = 4 (Benoit) and f_w = 2 (Debye) are displayed. This approach leads to the finding that aggregates are present with mean functionalities ranging from about 3.3 to 10 (Table 1). The highest concentration system for the SBdLi(2.6) family of headgroups is seemingly a mixture of dimers and tetramers. Modeling the data to the trimer aggregate led to a poorer fit than did the use of eq 4.

The accompanying change in functionality of the structures whose scattering contributions are found in the mid-Q (0.01 to 0.08 Å^{-1}) regime are listed in Table 1 along with the corresponding values of the equivalent SLi(2.6) systems. The latter system was found[20] to possess mixtures consisting of tetramer/dimer assemblys. This ratio was found to drift from 0.45 to 0.11 (f_w = 2.9−2.2) volume fraction of tetramers over the polymer concentration range 2.6−9.4%. As the data of Table 1 show, the intermediate-sized aggregates in the SBdLi(2.6) system can exhibit a mean functionality range of 3.3 to 10. This facet of the aggregation behavior for the butadienyllithium headgroup conflicts with the prevailing[2−15] model for propagation that requires the exclusive aggregation state of four. A similar scenario was found[20] for the styryllithium headgroup, where the simultaneous existence of dimers and tetramers is in violation of the same model requirements that certify the dimer as the exclusive aggregation state.

Figure 6 displays the star R_g and f_w (Table 1) as a function of polymer volume fraction for both headgroups. The relationships may be parametrized in terms of power laws; indicated by the straight lines in Figure 6 and numerically given in Table 2. All parameters for the two headgroups scale in a systematic fashion with the polymer concentration in terms of volume fraction. The R values describe the goodness of the fits. At present these power laws should be taken as phenomenological descriptions of the observed Φ dependencies. A physical interpretation remains missing.

Large Scale Aggregates. Having realized that the large scale aggregates coexist with the intermediate star like objects, we now iterate the description of the large structures on this basis. For this purpose we use the results of the Benoit description (Table 1) as an input and fit the additional low-Q intensity in terms of a single stage Beaucage mass fractal (first two terms in eq 2 with R_s = 0).

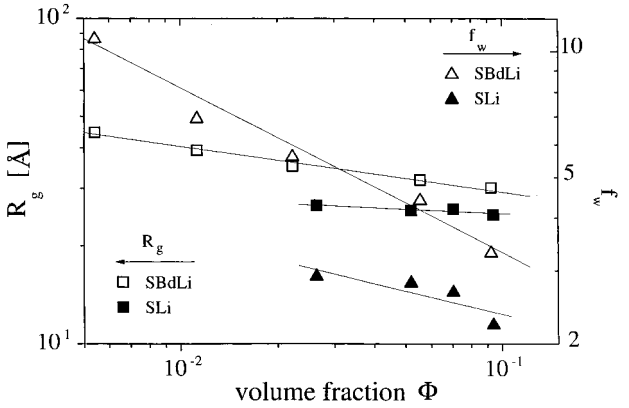

Figure 6. Dependence of star R_g and f_w (mean functionality) on Φ for the SLi and SBdLi headgroups.

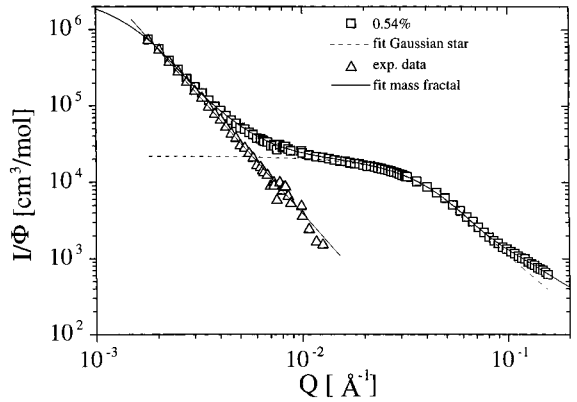

Figure 7. Fitting $I(Q)$ of the living polymer SBdLi(2.6) (□) headgroup with $\Phi = 0.54\%$ to the extended mass fractal form factor, eq 2, over the entire Q range. The fit of the Gaussian star is also shown where the mean f_w was assayed to be ~10. The residual intensity (△) is obtained following subtraction of the star intensity. This yields a universal power law with slope ≈3; which is the signature of a mass fractal. The two fitting techniques yield overlapping lines over the Q range of 2.0×10^{-2} to 7.0×10^{-2} Å^{-1}.

Table 2. Power Law Expressions for the Star R_g and Functionality as a Function of Polymer Volume Fraction

PSLi	$R_g = 23\ (\pm 1)\Phi^{-0.04(\pm 0.02)}$	$R = 0.91$
	$f_w = 1.6\ (\pm 0.6)\Phi^{-0.189\pm 0.08}$	$R = 0.84$
PSBdLi	$R_g = 21\ (\pm 1)\Phi^{-0.14(\pm 0.01)}$	$R = 0.99$
	$f_w = 1.3\ (\pm 0.5)\Phi^{-0.39(\pm 0.02)}$	$R = 0.99$

To picture the different contributions to the scattering function, Figure 7 displays experimental data for SBdLi at $\Phi = 0.54\%$. The mid- and high-Q data were fitted (dashed line) with the Gaussian star form factor[29] (eq 3). This form factor was then subtracted from the overall scattering at low-Q revealing the Q^{-3} power law from the large-scale aggregates existing over a large-Q range.

Table 3 presents the results of the fitting procedure. The parameters for R_g and P are in rough agreement with those displayed in Table 1. We note that amplitude factors are now to be interpreted as a product of the unknown volume fraction of the monomers within the large structures multiplied with their scattering volume V. With some exception for the different Φ these products $V\Phi_{\text{large scale}}$ are of the same order of magnitude. Given the large size for all Φ, this may indicate that in each instant only a very small roughly constant part (in absolute terms) of the total monomer population participates at the large objects.

Discussion

Parallel Findings. The aggregation findings show that electrostatic interactions exist in these self-assembling systems. In light of the antagonistic environment these essentially ionic[37−40] lipophobic headgroups are compelled to confront, it is not surprising that aggregation behavior reminiscent of ionomers[41] and surfactants[42] is encountered. In line with this behavior are the findings that the hydrocarbon insoluble benzyl- and allyllithium (the "tailless" versions of the species studied in ref 20 and this work) are known to form stacked arrays[43−45] in the solid state as do[46] [(trimethylsilyl)cyclopentadienyl]lithium; {[μ-η^5:η^5-$C_5H_4Si(CH_3)_3$]-Li}$_n$, 1,3 diphenylallyllithium[47] and [bis(trimethylsilyl)-methyl] lithium.[48] The aggregated array formed by the cyclopentadienyl compound has been characterized[46] as a highly ordered polymeric metallocene sandwich. ^{7}Li NMR studies[49] led to the conclusion that isoprenyllithium aggregates having $f_w > 4$ were formed. These examples demonstrate that lithium-based headgroups can form delocalized structures with the connate capacity to self-assemble into structures larger than tetramers. The intermolecular lithium−carbon interactions for allyllithium structures primarily involve the α-carbons of the aggregated headgroups.

In 1966 Makowski and Lynn[50] concluded from bulk viscosity measurements, that oligomeric butadienyllithium (initiated by *t*-BuLi in pentane) in the neat state developed association states beyond that of the tetramer. As shown in Figure 8, the Makowski−Lynn data demonstrates that the extent of aggregation and perhaps aggregate architectures are highly sensitive to tail length. The decrease in melt viscosity (squares in Figure 8) with increasing degree of polymerization, for the DP range of ca. 6−14, demonstrates the presence of aggregate breakup as chain DP increases. Under these conditions, the headgroup structure is seemingly constant.[51] For DP values >15 the viscosity begins to increase, demonstrating that the increase in chain length dominates the system viscosity. This does not rule out concurrent changes in aggregation states and/or aggregate architecture. The η_{ag}/η_d data (circles; Figure 8) exhibits a smooth drift toward the dimeric state ($\eta_{ag}/\eta_d = 1$) as chain length increases. This behavior can carry over into the solution state as a consequence of the lipophobic co-identity of the melt and solvent environments. Parallel changes in the melt state[52,53] and in solution[54] have also been observed for monofunctional zwitterionic-tipped polyisoprenes. This behavior is also supported by theory.[55]

These observations are, contrary to Szwarc's assessment,[15] in consonance with polymer brush behavior,[1] where increasing chain length can cause a decrease in brush functionality. The self-assembling behavior of BdLi headgroups received prior attention via concentrated solution (ca. 30% Φ polymer) viscosity measurements[56−58] involving high molecular mass chains (>10^5). That work consistently revealed the association state of two for the styryl- and dienyllithium headgroups.

Large Scale Structures. A careful analysis of the absolute scattering intensities shows that the picture of large fractal aggregation states build from smaller fractal subunits underlying the two-stage Beaucage form factor (eq 2) cannot be at the origin of the observed scattering patterns from the living polymer solutions. Instead, these solutions have to be considered as a mixture of dominating small aggregates which coexist

Table 3. Results of Fitting the *Q*-Range $Q \leq 0.08$ Å^{-1} to a Combination of the Beaucage Mass Fractal and the Benoit Star Form Factor[a] for the SBdLi and SLi[b] Headgroups

$10^2\Phi$	0.54	1.13	222/*2.64*	5.55/*5.20*	7.05	9.25/*9.40*
$G\Phi_{\text{large scale}}$	16300 ± 800	6000 ± 2000	9800 ± 1100/*3000*	5000 ± 900/*4100*	500	2700 ± 500/*1200*
R_g (Å)	1200 ±300	1600 ± 500	1500 ± 200/*1300*	1400 ± 200/*1400*	850	1000 ± 100/*1200*
P	3.0 ± 0.1	2.7 ± 0.2	2.8 ± 0.2/*3.0*	2.3 ± 0.1/*3.0*	3.1	1.9 ± 0.1/*2.8*

[a] The parameters for the Benoit star form factor were fixed to the values given in Table 1. [b] Italicized data (ref 20) are for SLi.

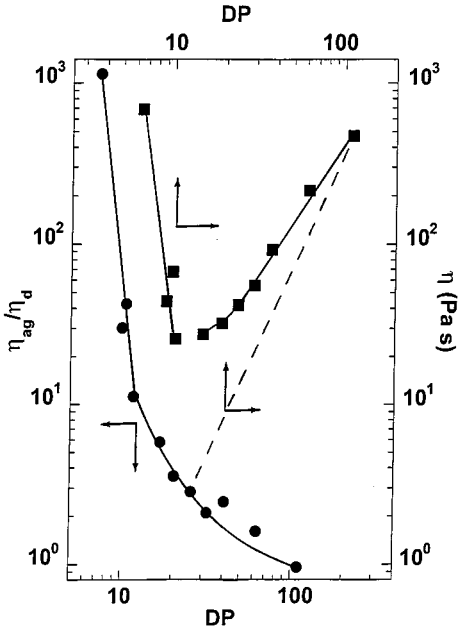

Figure 8. Makowski−Lynn viscosity data at 25 °C. The solid squares are the system viscosities (units of Pascal seconds) for the butadienyllithium headgroups as a function of the measured number-average degree of polymerization (DP) of the parent (singlet) chain. The solid circles denote the ratio of η_{ag}/η_d where η_{ag} denotes the aggregate viscosity and η_d that of the dimer. The dashed line is the dimer viscosity of the singlet chain DP ($\eta_d = 2.82 \times 10^{-3}$ DP$^{2.23}$; $R = 0.994$). The solid lines are simply guides for the eye.

with a very small number of large objects. Thereby, the monomer volume fraction participating at these large structures is below 1% of the total volume fraction in the solution. Furthermore, the scattering intensity from the large objects varies only moderately and unsystematically with the overall volume fraction Φ. This observation indicates that these large aggregates may be heterogeneously nucleated and do not manifest equilibrium properties of the living solution. From this consideration the intermediate star like structures evolve as the thermodynamic equilibrium aggregation states. Their concentration dependent aggregation behavior is discussed next.

"Thermodynamic Paradox". The aggregation behavior of the SLi(2.6) and SBdLi(2.6) headgroups show that for a given chain length the starlike objects approach the dimer aggregation state as the polymer concentration increases with the behavior being more pronounced for the diene derived unit. Thus, the aggregation number diminishes with increasing monomer volume fraction. Such a behavior is at variance with what is normally expected in aggregating systems where the critical micelle concentration (CMC) is reached via the act of dilution. This empirical behavior may be rationalized as follows:

(i) The enthalpy of the self-assembly event seems to favor larger aggregation states. This is in line with ab initio HF−SCF calculations[59] involving the lithium ester enolate of methyl isobutyrate and parallel calculations[60] involving allyllithium.

(ii) The chain growth event will create conformational entropy effects favoring smaller average aggregates. This influence would diminish beyond Φ*. Such conformational entropy effects are well-recognized for the case of polymer brushes,[1] where the chain-stretching effects lead to a loss of conformational chain entropy. Similar effects are expected in aggregates that become more crowded as the aggregation number increases.

(iii) The influence of translational entropy will cause a drive toward smaller average aggregation states with dilution.

(iv) Solvation effects of the ionic headgroups will modify the enthalpy of aggregate formation and at the same time reduce the translational entropy of the bound solvent molecules.

(v) Loss of monomer entropy during the polymerization event coupled with the potential for monomer solvation[61] of the headgroups. While this facet is not in play for our "post-polymerization" studies, it should not be neglected in the overall mechanistic picture.

The experimental observation of intermediate-sized aggregates, the average aggregation number of which diminishes with increasing concentration, requires that the loss of translational entropy (iii) of the headgroups, which is most pronounced at lower volume fractions, is counterbalanced by another source of entropy. This source, in the early stages of the polymerization event (low volume fraction) could only originate from solvation effects. Such solvation phenomenon may involve more solvent molecules per headgroup for the smaller aggregates, than for larger structures, as the consequence of increased openness of lesser aggregates headgroup structures (iv). This, together with the enthalpic drive to large aggregates (i), would favor the larger structures at low polymer concentrations (low conversions). The second source of entropy, arising from conformational effects becomes prominent at higher conversions. The reduction of aggregation at the larger concentrations then results from a decrease in translational entropy effects (iii and iv) which then leads to domination by the conformational entropic effects. This, in turn, encourages the formation of decreased aggregation states. The $\Delta H_{d,s}$ is calculated[61] to be 170 kJ for the allyllithium dimer (d) to singlet (s) event.

The scenario above requires a small change in aggregation enthalpy for each self-assembled cluster. This is acceptable since the coordination number of lithium can remain constant independent of the extent of association.

These observations indicate that the dimeric aggregate is not the preferred headgroup association state but that it simply denotes the balance between the headgroup packing preferences and the entropic considerations of the tethered high molecular mass tails.[55,62] This behavior is in agreement with the headgroup aggregation behavior findings reported in refs 43−48 and 56−58.

Conclusions

This SANS study has shown that the self-assembling capacities of the BdLi headgroup in benzene are more complex than the currently accepted propagation model permits. This is in agreement with previous conclusions[63] pertaining to these diene-based systems.The increase in polymer molecular mass and concentration seemingly leads to dimeric aggregates: a finding in accord with the melt[50] and concentrated solution viscosity results[56−58] and the SANS data for an SBdLi(33) chain.[64,65] The self-assembling behavior of these headgroups is similar to that observed for surfactant and ionomer systems and is compatible with generic polymer brush behavior[1]. Furthermore, the notion of aggregate unreactivity no longer seems tenable.[63,66−70] This receives support from the observations that freeze-dried SLi and SBdLi readily react[63,71,72] at room temperature with gaseous CO_2, dienes, and ethylene oxide. The aggregates are directly involved in these reactions since facile dissociation at room temperature is not feasible for vitrified polystyrene chains.

The feature of chain growth sets these self-assembling systems apart from their counterparts where the lipophilic tail is an invariant. It has been found[73,74] that increasing polymer chain length leads to a parallel increase in headgroup propagation reactivity. This is understandable in view of the sensitivity of aggregation states and, most likely, aggregate architecture upon chain length coupled with headgroup and polymer concentrations. This also explains the success[50,56,75−77] of the "seeding" procedure where oligomeric styryl- and dienyllithium chains are produced under conditions where complete initiation occurs. A further effect noted[74] was the variation in propagation reaction orders as the "seed" isoprenyllithium chain length decreased from a DP of ca. 500 to 25 over an active center range of ca. 10^{-4}−10^{-5}. Data exist[17] where the fractional reaction-order gradient increases with decreasing headgroup concentration. These combined features thus question the worth of fractional gradients as measures of aggregation states and their reliability as direct windows into the mechanistic characteristics of the anionic propagation event.

Acknowledgment. We wish to express our thanks to the reviewers for their comments and recommendations. These have led to improvements in the paper.

References and Notes

(1) Halperin, A.; Tirrell, M.; Lodge, T. P. *Adv. Polym. Sci.* **1992**, *100*, 31.
(2) Worsfold, D. J.; Bywater, S. *Can. J. Chem.* **1960**, *38*, 1981.
(3) Worsfold, D. J.; Bywater, S. *Can. J. Chem.* **1964**, *42*, 4884.
(4) Worsfold, D. J.; Bywater, S. *Macromolecules* **1972**, *5*, 393.
(5) Szwarc, M. In *Anionic Polymerization: Kinetics, Mechanisms and Synthesis*; McGrath, J. E., Ed., ACS Symposium Series 166; American Chemical Society: Washington, DC, 1981; p 1.
(6) Szwarc, M. *Adv. Polym. Sci.* **1983**, *49*, 1.
(7) van Beylen, M.; Bywater, S.; Smets, G.; Szwarc, M.; Worsfold, D. J. *Adv. Polym. Sci.* **1988**, *86*, 87.
(8) Szwarc, M.; van Beylen, M. *Ionic Polymerization and Living Polymers;* Chapman and Hall: New York, 1993.
(9) Szwarc, M. *Makromol. Chem., Macromol. Symp.* **1993**, *67*, 83.
(10) Bywater, S. *Prog. Polym. Sci.* **1994**, *19*, 287.
(11) Bywater, S. *Polym. Int.* **1995**, *38*, 325.
(12) Szwarc, M. *Ionic Polymerization Fundamentals*; Hanser/Gardner Publishers: Cincinnati, OH, 1996.
(13) Bywater, S. *J. Polym. Sci., Polym. Chem. Ed.* **1998**, *36*, 1065.
(14) Bywater, S. *Macromolecules* **1998**, *31*, 6010.
(15) Szwarc, M. *J. Polym. Sci., Polym. Chem. Ed.* **1999**, *37*, 873.
(16) Arest-Yakubovich, A. A. *J. Polym. Sci., Polym. Chem. Ed.* **1997**, *35*, 3613. This reference contains the misleading assertion that aggregate reactivity in anionic polymerization has been long recognized. While this is in accord with the views of many, e.g., see refs 37 and 66−70, it is incompatible with the stance of the authors of refs 2−15. They have for more than 3 decades consistently maintained that associated organolithium headgroups (alkyl, aryl, and allylic) in hydrocarbon solvents do not react with styrenic and diene monomers under polymerization conditions.
(17) Fetters, L. J.; Huang, J. S.; Stellbrink, J.; Willner, L.; Richter, D. *Macromol. Chem., Symp.*, **1997**, *121*, 1. This reference shows that some systems exhibit variable gradients over a 2−4 decade range in active center concentration; see Figures 2−4.
(18) Johnson, A. F.; Worsfold, D. J. *J. Polym. Sci., Part A* **1965**, *3*, 449.
(19) The kinetic order for the propagation reaction of butadiene was described[18] as "close to a $^1/_6$ dependence". This gradient reappeared[4] as $^1/_4$ (without explanation). Linear regression analysis reveals the gradient to be $^1/_5$.
(20) Stellbrink, J.; Willner, L.; Jucknischke, O.; Richter, D.; Fetters, L. J.; Huang, J. S. *Macromolecules* **1998**, *31*, 4189.
(21) Morton, M.; Fetters, L. J. *Rubber Chem. Technol.* **1975**, *48*, 359.
(22) Fetters, L. J.; Balsara, N. P.; Huang, J. S.; Jeon, H.; Almdal, K.; Lin, M. Y. *Macromolecules* **1995**, *28*, 4996.
(23) Zimm, B. H. *J. Chem. Phys.* **1948**, *16*, 1099.
(24) Beaucage, G.; Schaefer, D. *J. Non-Cryst. Solids* **1994**, *172−174*, 797.
(25) Beaucage, G. *J. Appl. Crystallogr.* **1995,** *28***,** 717.
(26) Beaucage, G. *J. Appl. Crystallogr.* **1996**, *29***,** 13
(27) Debye, P. *Phys. Colloid Chem.* **1947**, *51*, 18.
(28) Benoît, H. *J. Polym. Sci.*, **1953**, *11***,** 507.
(29) Daoud, M.; Stanley, H. E.; Stauffer, D. In *Physical Properties of Polymers Handbook;* Mark, J. E., Ed.; AIP: Woodbury, NY, 19XX; p 71.
(30) Fetters, L. J.; Hadjichristidis, N.; Lindner, J. S.; Mays, J. W. *J. Phys. Chem. Ref. Data* **1994**, *23*, 619.
(31) Huber, K.; Buntle, S., Lutz, P.; Burchard, W. *Macromolecules* **1985**, *18***,** 1461.
(32) Roovers, J. Private communication.
(33) This conclusion is based upon the combined (benzene and cyclohexane-Θ at 34 °C) power law behavior for polystyrene [η], R_g, and R_H: see ref 30.
(34) Richter. D.; Jucknischke, O.; Willner. L.; Fetters, L. J.; Lin, M.; Huang, J. S.; Roovers, J.; Toporowski, P. M.; Zhou, L. L. *J. Phys. IV, Colloq. C8, Suppl. J. Phys.* **1993,** *3*, 3.
(35) Willner, L.; Jucknischke, O.; Richter, D.; Farago, B.; Fetters, L. J.; Huang, J. S. *Europhys. Lett.* **1992**, *19*, 297.
(36) Willner. L.; Jucknischke, O.; Richter. D. Roovers, J.; Zhou, L. L.; Toporowski, P. M.; Fetters, L. J.; Huang, J. S.; Lin, M.; Hadjichristidis, N. *Macromolecules* **1994**, *27*, 3821.
(37) Weiss, E. *Angew. Chem., Int. Ed. Engl.* **1993**, *32*, 1501.
(38) Streitwieser, Jr., A.; Williams, Jr., J. E.; Alexandratos, S.; McKelvey, J. M. *J. Am. Chem. Soc.* **1976**, *98*, 4778.
(39) Streitwieser, A., Jr. *J. Organomet. Chem.* **1978**, *1−3*, 1.
(40) Bushby, R. J.; Steel, H. L. *J. Chem. Soc., Perkin Trans.* **1990**, *2***,** 1143. See also: *J. Organomet. Chem.* **1987**, *336*, C25.
(41) *Developments in Ionic Polymers*; Wilson, A. D., Prosser, H. J., Eds.; Applied Science: London, 1983; Vol. 1.
(42) *Structure and Dynamics of Strongly Interacting Colloids and Supramolecular Aggregates in Solution*; Chen, S.-H., Huang, J. S., Tartaglia, P., Eds.; NATO ASI Series C Mathematical and Physical Sciences 369; Kluwar Academic Publishers: Dordrecht, The Netherlands, 1992.
(43) Shumann, U.; Weiss, E.; Dietrich, H.; Madhi, W. *J. Organomet. Chem.* **1987**, *136*, 332.
(44) Beno, M. A.; Hope, H.; Olmstedt, M. M.; Power P. P *Organometallics* **1985**, *4***,** 117.
(45) Koster, H.; Weiss, E. *Chem. Ber.* **1982**, *115*, 3422.
(46) Evans, W. J.; Boyle, T. J.; Ziller, J. W. *Organometallics* **1992**, *11*, 3903.
(47) Boche, G.; Etzrodt, H.; Marsch, M.; Massa, W.; Baum, G.; Dietrich, H.; Mahdi, W. *Angew. Chem., Int. Ed. Engl.* **1986**, *25*, 104.
(48) Atwood, J. L.; Fjeldburg, T.; Lappert, M. E.; Longthi, T. N.; Shakir, R.; Thorne, A. J. *J. Chem. Soc., Chem. Commun.* **1984**, 1163.
(49) Boutillier, J.-M.; Favier, J.-C.; Hemery, P.; Sigwalt, P. *Polymer* ***1996****, 37*, 5197.
(50) Makowski, H. S.; Lynn, M. *J. Macromol. Sci.* **1966**, *1*, 443.

(51) It was found[50] that oligomeric (DP < 30) butadiene contained variable and high concentrations (up to ca. 47%) of 1,2 units. Under the conditions of the viscosity measurements, the headgroup concentrations ranged from ~0.15 to 4.7 M. ^{1}H NMR showed for ~0.5 M solutions in benzene that the active centers consisted of the cis and trans forms of the lithium-bearing headgroups. Terminal 1,2 structures were not found. (Bywater, S.; Worsfold, D. J.; Hollingsworth, G. *Macromolecules* **1972**, *5*, 389).
(52) Fetters, L. J.; Graessley, W. W.; Hadjichristidis, N.; Kiss, A. D.; Pearson, D. S.; Younghouse, L. B. *Macromolecules* **1988**, *21*, 1644.
(53) Shen, Y.; Safinya, C. R.; Fetters, L.; Adam. M.; Witten, T.; Hadjichristidis, N. *Phys. Rev. A* **1991**, *43*, 1886.
(54) Davidson, N. S.; Fetters, L. J.; Funk, W. G.; Graessley, W. W.; Hadjichristidis N. *Macromolecules* **1988**, *21*, 112.
(55) Brédas, J. L.; Chance, R. R.; Silbey, R. *Macromolecules* **1988**, *21*, 1633.
(56) Morton, M.; Fetters, L. J.; *J. Polym. Sci., Part A* **1965**, *3*, 449.
(57) Morton, M.; Fetters, L. J.; Pett, R. A.; Meier, J. F. *Macromolecules* **1970**, **3,** 3273.
(58) Al-Jarrah, M. M.; Young, R. N. *Polymer* **1980**, *21*, 119.
(59) Weiss, H., Yakimanski, A. V., Müller, A. H. E. *J. Am. Chem. Soc.* **1996**, *118*, 8897.
(60) Hommes, N. J. R.v. E.; Buhl, M.; Schleyer, P. v. R. *J. Organomet. Chem*. **1991**, *409*, 307.
(61) Korotkov first offered the concept of monomer complexation with lithium headgroups: Koroykov, A. A. *Angew. Chem*, **1958**, *70*, 85. In our ref 8, p 360; this notion is deemed to be correct whereas on the following page the opposite conclusion is reached.
(62) Wang, Z. G.; Safran, S. A. *J. Chem. Phys.* **1988**, *89*, 5323.
(63) Young, R. N.; Fetters, L. J.; Huang, J. S.; Krishnamoorti, R. *Polym. Int.* **1994**, *33*, 217.
(64) Reference 17, Figure 12.
(65) Fetters, L. J.; Huang, J. S.; Sung, J.; Willner, L.; Richter, D.; Lindner, P. in *Applications of Anionic Polymerization Research*; R. P. Quirk, Ed.; ACS Symposium Series 696; American Chemical Society: Washington, DC, 1998; p 38, Figure 7.
(66) See ref 50, p 463.
(67) Brown, T. L. *J. Organomet. Chem*. **1966**, *5*, 191.
(68) Sapse, A.-M.; Jain, D. C.; Raghavachari, K. In *Lithium Chemistry: A Theoretical and Experimental Overview*; Sapse, A.-M., Schleyer, P. v. R., Eds.; John Wiley and Sons: New York, 1995; p 45. Also see: Schleyer, P. v. R. *Pure Appl. Chem*. **1984**, *56*, 151.
(69) Smart, J. B.; Hogan, R.; Scherr, P. A.; Emerson, M. T.; Oliver, J. P. *J. Organomet. Chem*. **1974**, *64*, 1. This reference proposes a mechanism involving the direct reaction of monomer with aggregated headgroups that accounts for the cis and trans polydiene microstructures.
(70) Shamanin, V. V.; Melenevskaya, E. Yu.; Sgonnik, V. N. *Acta Polym*. **1982**, *33*, 175.
(71) Quirk, R. P.; Yin, J.; Fetters, L. J.; Kastrup, R. V. *Macromolecules* **1992**, *25*, 2262.
(72) Fetters, L. Unpublished observations.
(73) Bywater, S.; Worsfold, D. J. In *Recent Advances in Anionic Polymerization*; Hogen-Esch, T. E., Smid, J., Eds.; Elsevier: New York 1987; p 109.
(74) Madini, A. E.; Favier, J.-C.; Hemery, P.; Sigwalt, P. *Makromol. Chem., Rapid Commun.* **1990**, *11*, 329.
(75) Roovers, J. E. L.; Bywater, S. *Macromolecules* **1975**, *8*, 251.
(76) Lo, G. Y. S.; Otterbacher, E., W.; Gatzke, A. L.; Tung, L. H. *Macromolecules* **1994**, *27*, 2233.
(77) Yu, J. M.; Dubois, Ph.; Teyssié, Ph.; Jérôme, R. *Macromolecules* **1997**, *30*, 7356.

MA9817931